

Unique Axial Interaction of a Quadruply-Bonded Cr(II)–Cr(II) with Two Pt(II) Atoms in the Linearly Aligned Pt–Cr–Cr–Pt Supported by Four 6-Diphenylphosphino-2-pyridonate Ligands

Mitsuhiro Tanaka, Kazushi Mashima,* Masamichi Nishino,† Sadamu Takeda,*,†,# Wasuke Mori,†,## Kazuhide Tani,† Kizashi Yamaguchi,† and Akira Nakamura†

Department of Chemistry, Graduate School of Engineering Science, Osaka University, Toyonaka, Osaka 560-8531

† Department of Chemistry, Graduate School of Science, Osaka University, Toyonaka, Osaka 560-0043

(Received June 5, 2000)

Linearly aligned tetranuclear Pt(II)–Cr(II)–Cr(II)–Pt(II) complexes were prepared using a tridentate pyphos ligand (pyphos = 6-diphenylphosphino-2-pyridonate). The bonding between Cr(II) and Pt(II) was discussed on the basis of magnetic measurements. A dichromium complex, $[Cr_2(pyphos)_4]$ (**1**), was prepared by the reaction of $[Cr_2(OAc)_4]$ with the sodium salt of pyphos ligand. The complex **1** has four phosphorus atoms capable of holding transition metals at both of the axial positions of the Cr_2 moiety. Three tetranuclear Pt(II)–Cr(II)–Cr(II)–Pt(II) complexes, i.e., $[Cr_2Pt_2Me_4(pyphos)_4]$ (**2**), $[Cr_2Pt_2Cl_4(pyphos)_4]$ (**3**), and $[Cr_2Pt_2Cl_2Me_2(pyphos)_4]$ (**4**), have been prepared by the addition of the respective platinum species, $Pt^{II}Me_2$, $Pt^{II}Cl_2$, and $Pt^{II}MeCl$, to the axial positions of the Cr_2 moiety of **1**. Magnetic measurements of **1**–**4** together with a crystallographic study for the complexes **1** and **2** revealed that the quadruply-bonded Cr–Cr distance was delicately altered by the nature of the Pt atoms, i.e., the kind of substituents (Cl and/or Me) on the Pt atoms.

Dinuclear complexes with the metal–metal multiple bond have attracted much interest in views of their unique bonding nature and physical properties, since the first dinuclear complex bearing a metal–metal multiple bond, $[Re_2Cl_8]^{2-}$, was reported by Cotton et al.[1] In addition to the rhenium dinuclear complex, various transition metals, i.e., vanadium, chromium, molybdenum, tungsten, technetium, osmium and others have been used as components of the multiply-bonded M_2-type complexes.[2] Among these complexes, a quadruply-bonded Cr_2 complex is of particular interest: (1) the distance of the chromium–chromium bond depends on the bridging ligand, (2) axial ligands coordinated to the Cr_2 moiety sensitively affect the chromium-chromium bond distance, (3) the quadruple bond of the Cr_2 complex is relatively weaker than that found for Mo_2 or W_2, and hence (4) the temperature-dependent paramagnetism was often observed for some Cr_2 complexes in the solid state.[2–5] Thus, the chromium–chromium quadruple bond distance is widely ranging from about 1.83 Å to over 2.60 Å.[1] For a typical example of dichromium acetate complexes, elongation of the chromium–chromium bond and decrease of the singlet-triplet energy gap were induced by the coordination of organic ligands to the axial positions of the chromium–chromium bond. Temperature-dependence of the partial paramagnetism was indicated by variable-temperature NMR spectroscopy.[2]

We report herein the synthesis of three Cr_2Pt_2 tetranuclear complexes where two platinum(II) atoms with chloro and/or methyl ligands, in place of the organic donors in the above examples, coordinated to both of the axial positions of the dichromium moiety, so all four metals are linearly connected by four pyphos ligands (pyphos = 6-diphenylphosphino-2-pyridonate). The measurement of magnetic properties of these tetrametal complexes has been performed on the temperature-dependent NMR spectroscopy as well as the SQUID magnetometer. Results indicate that the substituents on the platinum(II) atoms delicately affected the bonding interaction between the platinum atoms and the chromium atoms. A part of this work has been the subject of a preliminary communication.[6]

Results and Discussion

Synthesis and Structure of $[Cr_2(pyphos)_4]$ (1). A starting dinuclear complex $[Cr_2(pyphos)_4]$ (**1**) was prepared in 67% yield from the sodium salt of the pyphos ligand and $[Cr_2(OAc)_4]$ in ethanol (Eq. 1), in a similar manner to the synthesis of a pyridonate complex $[Cr_2(mhp)_4]$ (mhp = 6-methyl-2-pyridonate) by the reaction of $[Cr_2(OAc)_4]$ with the sodium salt of mhpH (mhpH = 6-methyl-2-pyridone).[7] The $^{31}P\{^1H\}$ NMR spectrum of **1** in solution exhibited a broad singlet at δ –4.3 (fwhm = 660 Hz), indicating that all four phosphorus atoms are magnetically equivalent in solution and are free from the coordination of transition metals. The rather broad signal is owing to a partial contribution of a triplet state

Division of Chemistry, Graduate School of Science, Hokkaido University, Sapporo, 060-0810

Department of Chemistry, Faculty of Science, Kanagawa University, 2946 Tsuchiya, Hiratsuka , Kanagawa 259-1293

of the Cr_2 core, whose empty π^* orbitals interact with the filled lone pair orbitals of phosphorus atoms of the pyphos ligands.[8,9] The UV-vis spectrum of **1** showed a band of δ–δ^* transition at 455 nm, the same value as that of the typical quadruply-bonded Cr–Cr, e.g., $[Cr_2(dfm)_4]$ (dfm = di-*p*-tolylformamididinate) (445 nm).[10]

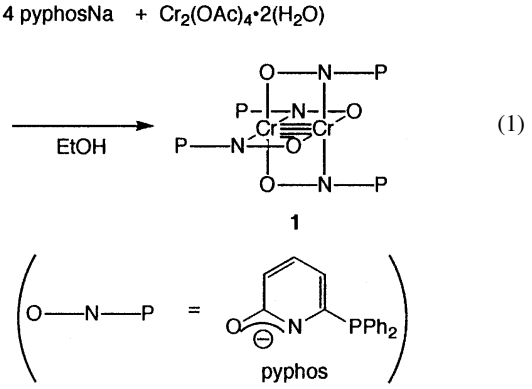

(1)

Figure 1 shows the dinuclear structure of **1**. Selected bond distances and angles for **1** are summarized in Table 1. It is a notable structural feature that **1** has two *trans*-arranged phosphine atoms capable of coordinating to transition metals at both sides of the Cr_2 core. The distance (2.015(5) Å) of the quadruple Cr–Cr bond is longer than that reported for $[Cr_2(dmhp)_4 \cdot 0.5(O_3C_6H_{14})]$ (dmhp = 2,4-dimetyl-6-hydroxypyrimidinate; $O_3C_6H_{14}$ = diglyme) (1.898(3) Å),[11] $[Cr_2(dmhp)_4 \cdot O_3C_6H_{14}]$ (1.907(3) Å),[11] $[Cr_2(chp)_4]$ (chp = 6-chloro-2-pyridonate) (1.955(2) Å),[12] and $[Cr_2(mhp)_4]$ (1.889(1) Å),[7] but shorter than that (2.288(2) Å) of $[Cr_2(OAc)_4]$.[13] It is normal that the average Cr–O distance (1.95 Å) is shorter than the average Cr–N bond distance (2.08 Å). Dihedral angles of O1–Cr1–Cr2–N2 (12.4(7)°), O2–Cr1–Cr2–N2 (10.3(7)°), O3–Cr1–Cr2–N2 (6.8(7)°), and O4–Cr1–Cr2–N4 (10.2(7)°, av 9.9°) are larger than those found for dichromium pyridonate complexes, $[Cr_2(dmhp)_4 \cdot 0.5(O_3C_6H_{14})]$ (av 2.1°),[11] $[Cr_2(dmhp)_4 \cdot O_3C_6H_{14}]$ (av 0.6°),[11] $[Cr_2(chp)_4]$ (av 4.3°),[12] $[Cr_2(mhp)_4]$ (av 2.0°).[7] The distortion of **1** may be attributed to the bulkiness of diphenylphosphino substituent at 6-position of the pyridonate moiety.

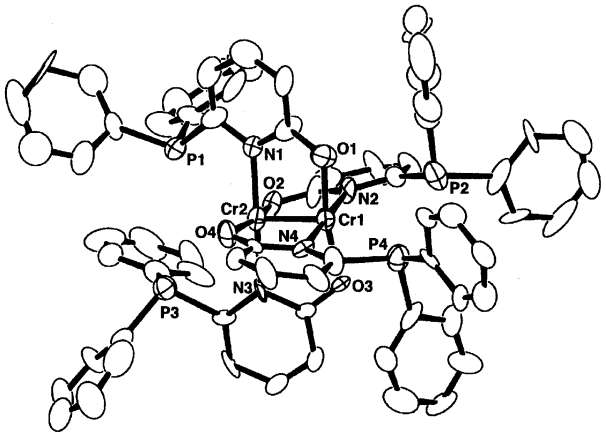

Fig. 1. A drawing of **1** with the atom labeling scheme. Hydrogen atoms are omitted for clarity.

Table 1. Selected Bond Distances (Å) and Angles (Degree) for **1**

Distances (Å)			
Cr1–Cr2	2.015(5)	Cr1–O1	1.93(2)
Cr1–O3	1.94(1)	Cr2–O2	2.00(2)
Cr2–O4	1.94(2)	Cr1–N2	2.12(2)
Cr1–N4	2.09(2)	Cr2–N1	2.04(2)
Cr2–N3	2.07(2)	P1···P3	3.88
P2···P4	3.91		
Angles (Degree)			
O1–Cr1–O3	167.8(7)	N2–Cr1–N4	179.0(8)
O2–Cr2–O4	167.4(7)	N1–Cr2–N3	177.1(8)
O1–Cr1–N2	92.4(7)	N2–Cr1–O3	90.4(7)
O3–Cr1–N4	88.9(7)	N4–Cr1–O1	88.4(7)
N1–Cr2–O2	90.3(7)	O2–Cr2–N3	86.8(7)
N3–Cr2–O4	92.0(7)	O4–Cr2–N1	90.7(7)

Synthesis of $[Cr_2Pt_2Me_4(pyphos)_4]$ (2), $[Cr_2Pt_2Cl_4(pyphos)_4]$ (3) and $[Cr_2Pt_2Cl_2Me_2(pyphos)_4]$ (4). Treatment of **1** with two equiv. of $[PtMe_2(cod)]$ (cod = 1,5-cyclooctadiene) in THF afforded $[Cr_2Pt_2Me_4(pyphos)_4]$ (**2**) in quantitative yield (Eq. 2). During the reaction course, the geometry of the four pyphos ligands changed from a *trans*-fashion to a *cis*-one, which might be attributed to the *trans* influence of the methyl group bound to the platinum atom. Alternatively, the complex **2** was derived by the reaction of $[PtMe_2(pyphosH)_2]$ with $[Cr_2(OAc)_4]$ in the presence of NaOMe in THF. In sharp contrast to the dichromium complex **1**, the tetranuclear Cr_2Pt_2 complex **2** did not exhibit any signals in the $^{31}P\{^1H\}$ NMR spectrum in solution. The formation of a paramagnetic species was a result of a partial disruption of the quadruple Cr–Cr bond through the interaction with two $PtMe_2$ moieties. A similar partial contribution of the open-shell $(\sigma)^2(\pi)^4(\sigma)^1(\sigma^*)^1$ configuration on a Cr_2 bond has been reported; the Cr–Cr distance of $[Cr_2(OAc)_4(L)_2]$ (L = MeOH, H_2O, pyridine, and MeCN) was found to depend on the kind of donor ligands L at the axial positions of the Cr–Cr bond, and the elongation of the Cr–Cr bond decreases the singlet–triplet separation.[2] Indeed, two $PtMe_2$ moieties can interact attractively with Cr_2 core, forming Pt–Cr dative bonds and resulting in the elongation of Cr–Cr bond.

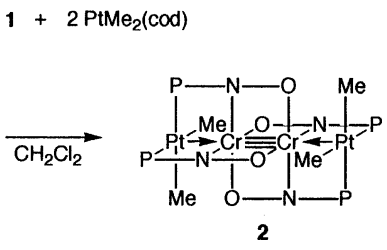

(2)

The bonding nature of **2** has been verified by the X-ray crystallographic study. Figure 2 shows the ORTEP diagram of **2** and the selected bond distances and bond angles are summarized in Table 2. The notable feature is the significant elongation of the Cr–Cr bond distance (2.389(9) Å) as expected by NMR measurement, longer by 0.374 Å than that of **1**; the distance is comparable to those (2.329(2)–2.396(2) Å) of

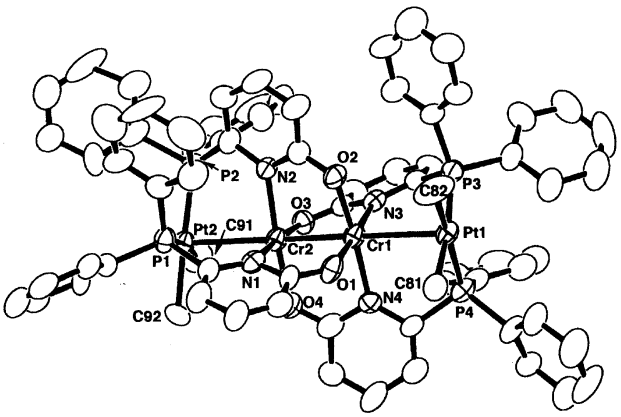

Fig. 2. A drawing of **2** with the atom labeling scheme. Hydrogen atoms are omitted for clarity.

Table 2. Selected Interatomic Distances (Å) and Angles (Degree) for **2**

Distances (Å)			
Cr1–Cr2	2.389(9)	Cr1–Pt1	2.806(9)
Cr2–Pt2	2.811(3)	Pt1–C81	2.12(5)
Pt2–C82	2.088(9)	Pt1–P3	2.282(7)
Pt1–P4	2.304(4)	Pt2–P1	2.313(3)
Pt2–P2	2.261(5)	Cr1–O1	1.96(2)
Cr1–O2	1.95(3)	Cr2–O3	1.99(3)
Cr2–O4	1.98(3)	Cr1–N3	2.14(5)
Cr1–N4	2.145(2)	Cr2–N1	2.16(3)
Cr2–N2	2.12(2)		
Angles (Degree)			
Pt1–Cr1–Cr2	178.87(3)	Cr1–Cr2–Pt2	178.1(2)
Cr1–Pt1–C81	92(1)	Cr1–Pt1–C82	97(2)
Cr1–Pt1–P3	83.2(3)	Cr1–Pt1–P4	86.5(2)
Cr2–Pt2–C91	97(1)	Cr2–Pt2–C92	96.08(8)
Cr2–Pt2–P1	85.38(6)	Cr2–Pt2–P2	83.3(1)
O1–Cr1–N3	176(1)	O2–Cr1–N4	176.1(9)
O3–Cr2–N1	175(15)	O4–Cr2–N2	176(1)
O1–Cr1–O2	91.1(6)	O2–Cr1–N3	90.3(6)
N3–Cr1–N4	92.1(3)	N4–Cr1–O1	86.2(4)
N1–Cr2–N2	93(1)	N2–Cr2–O3	91(1)
O3–Cr2–O4	90(1)	O4–Cr2–N1	86(1)

$[Cr_2(OAc)_4(L)_2]$ where L = H_2O,[14] Py,[15] MeOH,[2] and MeCN.[2] Although the interatomic distances (2.806(9) and 2.811(3) Å) between the platinum atom and the chromium atom are longer than the sum (2.6 Å) of Cr and Pt atomic radii, they are still regarded as having dative Pt–Cr bonds. Similar metal-to-metal dative bonds containing group 10 metals, even though their distances are too long to form direct metal-to-metal bonds, have already been reported.[16–20] Furthermore, the attractive interaction between the Pt atom and the Cr atom is evidently observed as the shift of the Pt atom toward the chromium atom by 0.03 Å from the least square plane consisted of two methyl ligands and two phosphorus atoms. The angles of Cr–Pt–P [83.2(3), 86.5(2), 85.38(6) and 83.3(1)°] are acute, while the angles of Cr–Pt–Me [92(1), 97(2), 97(2) and 96.08(8)°] are obtuse. This is the first example where transition metals act as the axial donors to the quadruple Cr—Cr bond to elongate it, though the donor property of the metal atoms in square planar complexes has often been reported.[16,17,20–24]

On the other hand, we observed the completely opposite effect of the chloride ligand on the platinum atom. A tetranuclear Cr_2Pt_2 complex $[Cr_2Pt_2Cl_4(pyphos)_4]$ (**3**) was prepared by the reaction of complex **1** with two equiv. of $PtCl_2(cod)$ (Eq. 3). The $^{31}P\{^1H\}$ NMR spectrum of the chloro derivative **3** in solution displayed a sharp singlet at σ 12.6 with a satellite due to platinum nucleus (3590 Hz), indicating that **3** is a typical diamagnetic complex. Thus, the quadruple Cr–Cr bond was found to be highly sensitive to the electron donating property of the ligand on the Pt(II) atom.

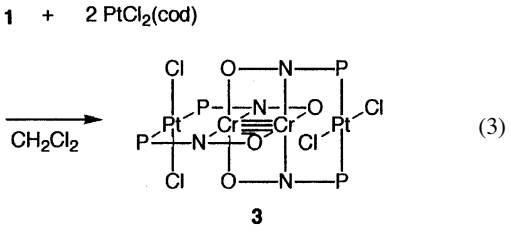

(3)

In order to elucidate the influence of substituents on the platinum atoms to the Cr–Cr bond, we prepared a complex $[Cr_2Pt_2(pyphos)_4Cl_2Me_2]$ (**4**) in which each platinum atom has both methyl and chloro ligands. The tetranuclear complex **4** was obtained by the slow diffusion of THF solution of [PtClMe(cod)] into the dichloromethane solution of **1**. The crystallization afforded **4** as orange needles in quantitative yield upon standing over a couple of weeks. Complex **4** is thoroughly insoluble in common organic solvents except for dichloromethane (0.4 mg mL^{-1}). Mass spectrum and elemental analysis supported the formulation of **4**, but NMR spectroscopy in solution did not exhibit any signal, indicating that at least one methyl ligand on the platinum atom caused the elongation of the Cr–Cr bond to result in the formation of paramagnetic species.

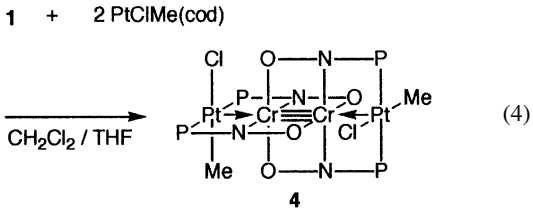

(4)

Magnetic Properties of Dinuclear and Tetranuclear Complexes 1–4. Measurement of the Solid State High-resolution ^{31}P NMR of Complexes 1 and 2. Magic angle spinning (MAS) averages anisotropy of the chemical shift and dipole interactions to provide the isotropic shift of the ^{31}P NMR absorption line. The observed isotropic shift in ppm consists of the Fermi contact term, the pseudo contact term (dipole interaction between nuclear and electron spins) and the temperature independent diamagnetic term as follows:

$$\delta_{iso} = \delta_{Fermi} + \delta_{Pseudo} + \delta_{dia} \quad (5)$$

$$\delta_{\text{Fermi}} = \frac{\mu_B}{3k_BT}\cdot\frac{A_{\text{Fermi}}}{\gamma/2\pi}\cdot\left(\frac{g_{xx}+g_{yy}+g_{zz}}{3}\right)\cdot[S(S+1)\cdot F(J,T)], \quad (6)$$

$$\delta_{\text{pseudo}} = \frac{\mu_B^2}{18k_BTr^3}\cdot\{[2g_{zz}^2-(g_{xx}^2+g_{yy}^2)](3\cos^2\theta-1) - 3(g_{yy}^2-g_{xx}^2)\sin^2\theta\cos 2\Omega\}[S(S+1)\cdot F(J,T)] \quad (7)$$

where A_{Fermi} is the Fermi contact coupling constant of the nucleus of interest in Hz and is proportional to the electron spin density induced by Cr(II)–Cr(II) core at the nucleus.[25,26] δ_{dia} is the shift that the same nuclear spin would have in an equivalent diamagnetic environment. The function $F(J,T)$ expresses a Boltzmann distribution among the electron spin states of Cr(II)–Cr(II) core. Pseudo contact term shows the same temperature dependence as the Fermi contact term in the case that zero field splitting is negligible. Then Eqs. 5–7 can be expressed by

$$\delta_{\text{iso}} = \delta_{\text{dia}} + \frac{\mu_B}{3k_BT}\cdot\frac{A}{\gamma/2\pi}\cdot[S(S+1)\cdot F(J,T)]. \quad (8)$$

The experimentally determined hyperfine-coupling constant A consists of the two terms. The anisotropy of the g-tensor contributes to the pseudo contact term. The magnetic interaction J can be determined from the temperature dependence of $F(J,T)/k_BT$.

The temperature variation of the proton decoupled ^{31}P MAS/NMR spectra of the dinuclear complex **1** is shown in Fig. 3. The width of the absorption line became sharper as the temperature was decreased and at least two peaks were distinguished below 215 K. Nonequivalent ^{31}P atoms were attributed to crystallographically nonequivalent sites in a complex in the crystalline phase, as indicated by X-ray diffraction experiments (*vide supra*). Temperature dependence of the ^{31}P resonances is very similar to that seen for the proton peak of $[Cr_2(O_2CCH_3)_4(MeOH)_2]$ in solution[2] and can be explained by the Boltzmann distribution among the different spin states of coupled system of two $S = 2$ ions Cr(II)–Cr(II).

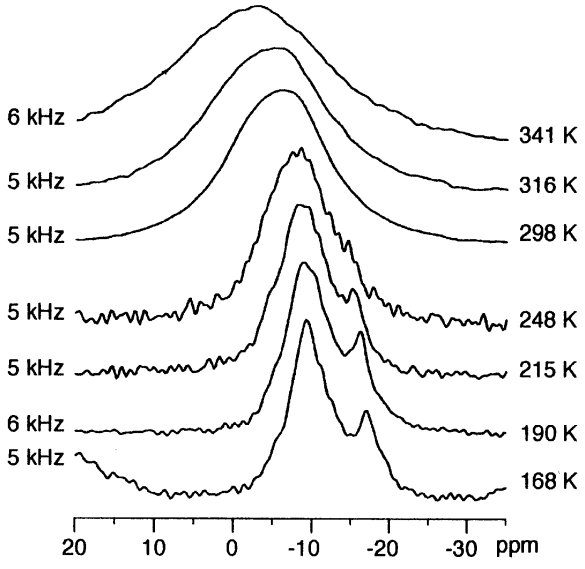

Fig. 3. Temperature dependence of proton decoupled ^{31}P MAS NMR spectrum of **1** in the crystalline phase. Magic angle spinning (MAS) speed and temperature are indicated in the Figure.

From the basic theories of magnetism and of NMR of paramagnetic materials,[27–29] one can derive the term $[S(S+1)\cdot F(J,T)]$ in Eq. 8 to describe satisfactorily the variation of the NMR shifts with temperature,[29]

$$[S(S+1)\cdot F(J,T)] = \frac{(6e^{2J/kT}+30e^{6J/kT}+84e^{12J/kT}+180e^{20J/kT})}{(1+3e^{2J/kT}+5e^{6J/kT}+7e^{12J/kT}+9e^{20J/kT})}, \quad (9)$$

where Heisenberg's model for the magnetically coupled $S = 2$ ions system and the same hyperfine-coupling constant for different spin states are assumed. The value $E = -2J$ is singlet-triplet energy splitting defined by the spin Hamiltonian $H = -2J\hat{S}_1\cdot\hat{S}_2$. Here it is noted that ab initio calculations indicated the plausibility of applying the Heisenberg's model to the Cr(II)–Cr(II) core. Ab initio CASCI and CASSCF calculations, which include electron correlations, were performed for Cr(II)–Cr(II) dinuclear complexes and the energy levels of different spin states were examined, i.e. $E(s=0)$, $E(s=1)$,and $E(s=2)$. The calculated spin energy scheme almost coincides with the assumption of Heisenberg's model, at least for the lower spin states, $E(s=1)-E(s=0) = -2J$, $E(s=2)-E(s=1) = -4J$, and $E(s=3)-E(s=2) = -6J$, for Cr(II)–Cr(II) bond distances between 2.0 and 3.0 Å.[30–32] Values of magnetic interaction J and hyperfine-coupling constant A can be determined by fitting the ^{31}P MAS NMR shift data with Eqs. 8 and 9. Solid and broken curves in Fig. 4 depict the result of fitting for the two peaks in Fig. 3. The accurate value of J was determined from the lower field peak (●) and the same value of J was used for the higher field peak (▲), since the magnetically coupled Cr(II)–Cr(II) core is common for the crystallographically inequivalent ^{31}P sites in the complex. Since singlet-triplet energy level splitting in this complex is large ($E = 1080$ cm^{-1}) compared with thermal energy below 350 K, the thermal population in higher spin states than quintet state is very small and contributes little to

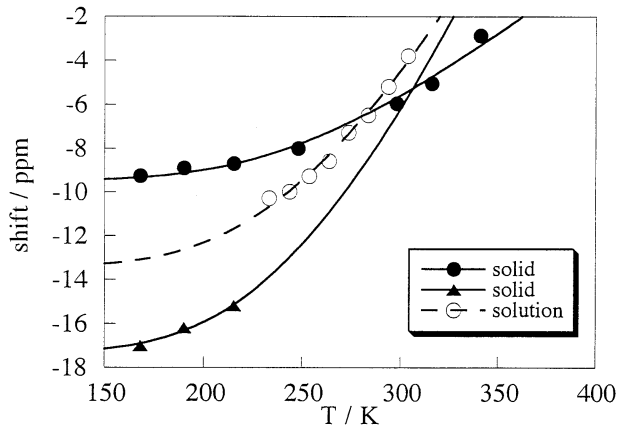

Fig. 4. Temperature dependence of the ^{31}P NMR shifts of **1** in the crystalline phase (● and (▲) and in the $CDCl_3$ solution (○).

the observed variation of the NMR shift with temperature. Analysis of NMR shift of **1** by using a singlet-triplet model gave the same value of J. The derived values are summarized in Table 3 together with those for the complex in $CDCl_3$ solution. In solution single peak of ^{31}P NMR absorption was observed over the temperature region investigated, as shown in Fig. 5. The freezing point of the solvent in which the complex is soluble determines the low temperature limit of the measurement. The observed shift (○) and its temperature variation in solution are in between the two resonance lines for the solid state (● and ▲), as depicted in Fig. 4. This result indicates that crystallographically nonequivalent sites of ^{31}P in the complex become equivalent in solution. Independent fitting for the solution NMR gave the value $J = -530$ cm^{-1} which is the same value as that observed in the solid state within error.

Temperature dependences of the proton decoupled ^{31}P MAS/NMR spectra were also measured for the complex **2** in the solid state and are shown in Fig. 6. Two peaks were distinguished above room temperature, corresponding to the crystallographically nonequivalent ^{31}P sites, as in the case of **1**. The ^{31}P NMR spectrum showed a sudden change between 256 and 306 K and the temperature dependent spectra were reversibly reproduced. This result suggests that a structural phase transition occurs between 256 and 306 K and the ^{31}P NMR shift reflects sensitively the change of the local structure of the complex. In the lower temperature phase, the NMR shifts of all

Table 3. Magnetic Interaction of Cr(II)–Cr(II) Determined by Variable Temperature ^{31}P MAS NMR

Complex	$-J$ (cm^{-1})	A/h (MHz)	δ_{dia} (ppm)
1 (solid)	540	+7.1, +20	−9, −17
1 (solution)	540	+16	−13
2 (solid)	ca. 10[a)]	ca. −0.2[a)]	ca. +80[a)]

a) These values are order estimate for the low temperature phase. The phase transition limited the number of data points for estimating J, A, and δ_{dia}.

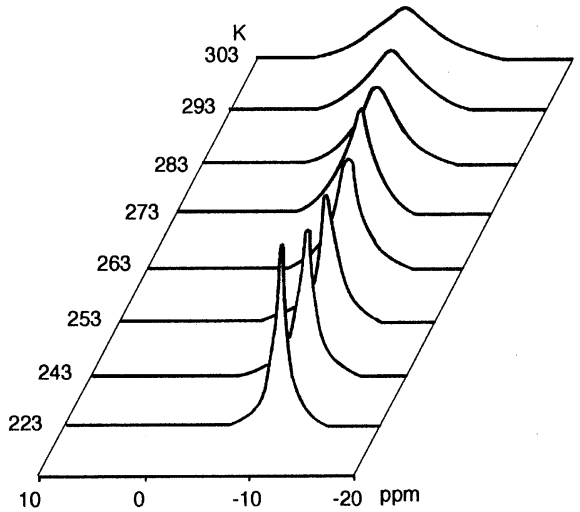

Fig. 5. Variable temperature $^{31}P\{^1H\}$ NMR spectra of **1** in $CDCl_3$ solution.

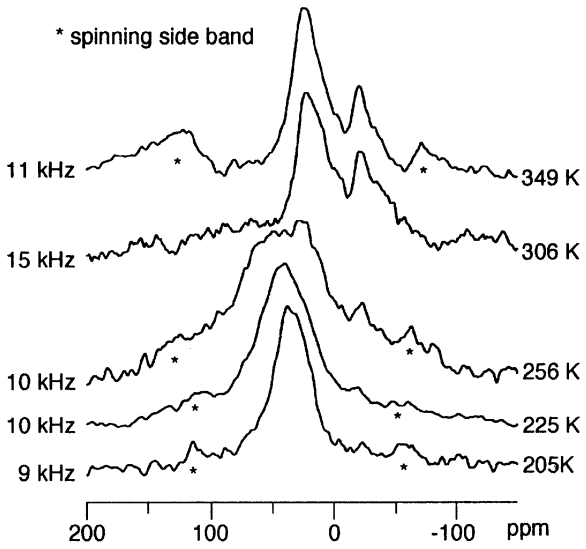

Fig. 6. Temperature dependence of proton decoupled ^{31}P MAS NMR spectrum of **2**. Magic angle spinning (MAS) speed and temperature are indicated in the Figure. Asterisk indicates spinning side bands. Phase transition occurs between 256 and 306 K.

^{31}P nuclei become similar to each other and distortion of the complex **2** in this phase is smaller compared with that in the higher temperature phase. For both higher and lower temperature phases of **2**, it is noted that the line width of the NMR signals is large compared with that for **1**, indicating that antiferromagnetic coupling between the two Cr(II) ions of **2** is small and that thermal populations in the triplet and higher spin states are large. Determination of the accurate value of J for **2** from the temperature dependent NMR shift is difficult because of the phase transition. However, the order of J value could be estimated to be J~10 cm^{-1} from the temperature dependence of NMR shift in the low temperature phase. The value of J is consistent with magnetic susceptibility measurements and is much smaller than that of **1**.

Magnetic Measurement of Complex 1–4 by a SQUID Magnetometer. The temperature-dependence of the paramagnetism has been used to estimate the separation between the singlet ground state and the lowest triplet state (an open-shell $(\sigma)^2(\pi)^4(\delta)^1(\delta^*)^1$ configuration on Cr_2 bond). The temperature dependence of magnetic susceptibilities of complexes **1–4** was measured by a SQUID magnetometer (Quantum Design MPMS-5S).

The data of **1** (Fig. 7) have been analyzed in terms of the theoretical equation for a magnetically coupled system of two $S = 2$ cores corrected by paramagnetic impurity (Cr(III) impurities) (Eq. 10) with $g = 1.8$, $J = -280$ cm^{-1}, $p = 0.04$.

$$\chi_A = \frac{Ng^2\mu_B^2}{kT}\cdot\frac{e^{2x} + 5e^{6x} + 14e^{12x} + 30e^{20x}}{1 + 3e^{2x} + 5e^{6x} + 7e^{12x} + 9e^{20x}}\cdot(1-p) + \frac{5Ng^2\mu_B^2}{4kT}\cdot p \qquad (10)$$

$$x = \frac{J}{kT}$$

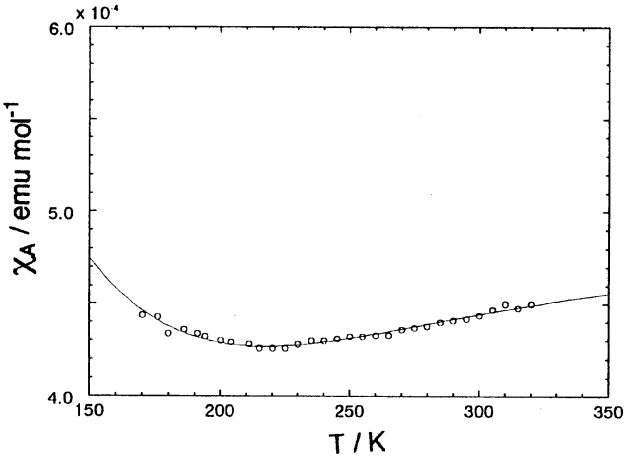

Fig. 7. Temperature dependence of magnetic susceptibility χ_A for **1**.

In the same manner, magnetic properties of complexes **2** (Fig. 8) and **4** (Fig. 9) were measured. The results are summarized in Table 4.

The intradimer exchange integral J of **1** (–280 cm^{-1}) is similar to those of the acetate complexes, although its Cr–Cr distance (2.015 Å) is smaller than those (2.3–2.5 Å) of the acetate complexes.[2,15,33–36] The intradimer exchange interaction (J) of **2** (–29 cm^{-1}) is much smaller than that of **1**, corresponding to a much longer Cr–Cr distance (2.389 Å) for **2** than that for **1**. The relationship of magnetic interaction J and chromium–chromium bond distance is shown in Fig. 10. The J values of complexes **1** and **2** were different from those of dichromium carboxylates, because the kind of the bridging ligand, pyridonate or acetate, might contribute to the J values, however, a decreasing tendency of the singlet-triplet gap with elongation of the Cr–Cr bond was observed. The J value of **4** (–52 cm^{-1}) is comparable to that of **2**. Thus, the Cr–Cr distance of **4** was likely to be elongated in the same order as that found for **2**. On the other hand, no paramagnetism was observed in the case of **3**, as

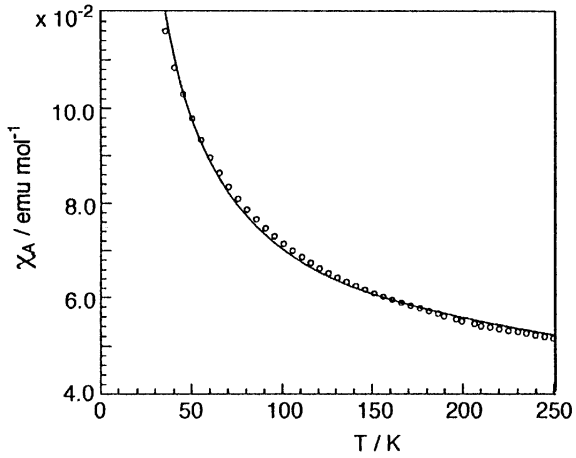

Fig. 8. Temperature dependence of magnetic susceptibility χ_A for **2**.

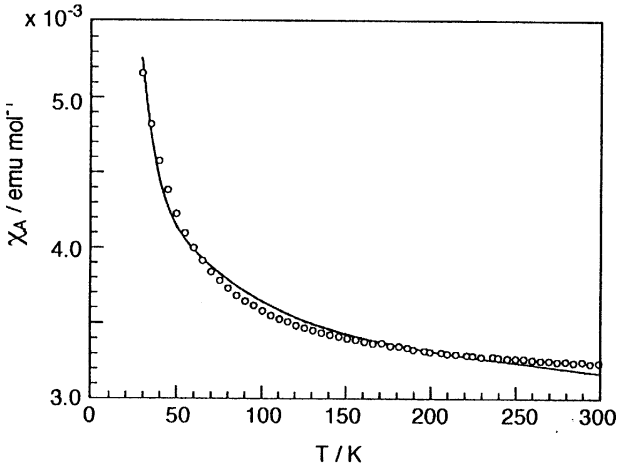

Fig. 9. Temperature dependence of magnetic susceptibility χ_A for **4**.

Table 4. Magnetic Measurement of Complexes **1–4** by a SQUID Magnetometer

Complex	g	$-J$ (cm^{-1})
1	1.8	> 280
2	1.8	29
3	—	diamagnetic
4	1.9	52

noted already by NMR measurements in solution, indicating that the Cr–Cr distance of **3** is shorter than those found for **1**, **2**, and **4**. In partial support of this result, the X-ray analysis of the molybdenum anologue of **3**, $[Mo_2Pt_2Cl_4(pyphos)_4]$ (**5**, Scheme 1), showed that the two platinum atoms at both axial positions of the Mo_2 core slightly deviated outside from the normal position in the square planar geometry.[37]

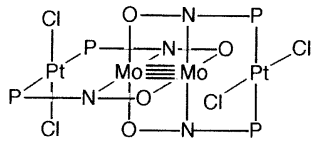

5

Scheme 1.

Bonding Discription. To estimate the effect of elongation of Cr–Cr bond and the effect of addition of terminal metal atoms on the J value, ab initio calculations were performed for linearly aligned naked tetrametal system Ni(II)–Cr(II)–Cr(II)–Ni(II) without ligands, where Ni(II) was used instead of Pt(II) for the simplicity of the calculation.[30–32] As shown in Fig. 10, the absolute value of J also decreased almost exponentially as Cr(II)–Cr(II) bond distance increased, where the Ni(II)–Cr(II) distance is fixed to 2.0 Å. Such a relation has been pointed out by Cotton et al. from the solution NMR experiments on dichromium carboxylate complexes with a Cr(II)–Cr(II) core.[2] The bond distance of Cr(II)–Cr(II) in **4**, which is presently unknown, is considered to be similar to that

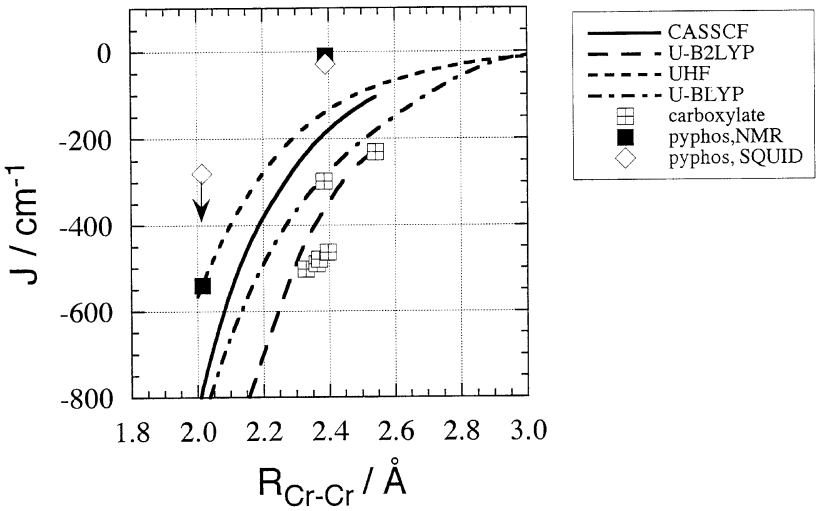

Fig. 10. Variation of antiferromagnetic exchange interaction J with intermetallic bond length R_{Cr-Cr} of Cr(II)-Cr(II). ■: Experimental values determined by ^{31}P MAS NMR for **1** and **2**. ◇: Experimental values determined by SQUID for **1** and **2**. ⊞: Dinuclear Cr(II)-Cr(II) complexes with carboxylate ligands. Smooth curves are molecular orbital calculations with different methods. [30–32]

in the complex **2**, since the observed J value of **4** is the same order as J of **2**. The ab initio calculations indicated that the intermetallic bond between Cr(II) and Ni(II) in the linearly aligned tetrametal system Ni(II)···Cr(II)–Cr(II)···Ni(II) is weak, while the intermetallic bond between Cr(II) and Ni(I) in the analogue Ni(I)–Cr(II)–Cr(II)–Ni(I) becomes strong. A similar trend might be expected for electronically isostructural $Cr(II)_2Pt_2$ systems.

For the discussion of the intermetallic bond between Cr(II) and Pt(II), it is important to investigate the interaction between Cr(II) and Pt(II) in complex **2**. The interaction may be estimated from the hyperfine coupling constants A of ^{31}P obtained in this study. Although no data of anisotropy of g values are available for **1** and **2**, we can estimate a dominant contribution of Fermi contact term for the observed hyperfine coupling constants of 7.1 and 20 MHz for **1** as follows. Supposing that the hyperfine coupling constants of 7.1 and 20 MHz for **1** are determined by dipole (pseudo contact) interaction between Cr and P , we calculate that the term of $[2g_{zz}^2 - (g_{xx}^2 + g_{yy}^2)]$ in Eq. 7 must be the order of 100 for 3.2–3.3 Å of Cr–P distance of **1**. This value seems to be unrealistically large; the dominant contribution for the hyperfine coupling constants of **1** is the Fermi contact term. The Cr–P distances of 3.4–3.5 Å of **2** are slightly larger than those of **1**. The hyperfine coupling constants of ^{31}P of **1** are large and positive as listed in Table 3. The positive sign suggests that the electronic spins induced at the ^{31}P nucleus has the same sign as the electronic spin on the Cr(II)–Cr(II) core. The electronic spins on ^{31}P of the pyphos ligand is induced through the bonding path of Cr–N–C–P. This spin induction path is almost the same for complexes **1** and **2**. However, the electronic spin induced on ^{31}P of **2** is much smaller than that of **1**. This result suggests that an additional spin induction path, i.e. Cr–Pt–P, exists and operates to bring about the negative spins on the ^{31}P of the pyphos ligands. The two conflicting effects may almost cancel the electronic spin density at the ^{31}P, and consequently the hyperfine coupling constant A of **2** is small and negative, as listed in Table 3. Although the distances 2.806(9) and 2.811(3) Å between Cr(II) and Pt(II) of **2** determined by X-ray diffraction are longer than the sum of Cr and Pt atomic radii and no strong bonding is expected between Cr(II) and Pt(II), a significant interaction, which mediates a spin induction, exists between Cr(II) and Pt(II).

Conclusion

We have demonstrated that the Cr–Cr bond of the $Cr(II)_2$-$Pt(II)_2$ complexes (**2–4**) can be controlled by the kind of substituents on the platinum(II) atoms. Paramagnetic properties of **2** and **4** have been elucidated by the solid state NMR measurement and the magnetic measurement (SQUID), whereas **3** was found to be diamagnetic. This is the first example of the Cr–Cr bond elongation induced by metal species placed at the axial positions of the Cr_2 core, though the Cr–Cr bond elongation caused by axial coordination of organic ligands has been reported. Additionally, our findings are in sharp contrast to the observation by Cotton et al., who found no interaction between axial Cu(I) metals with internal Cr_2 core of Cu–Cr–Cr–Cu tetrametal cluster supported by the anion of 2,6-di(phenylimino)piperidine.[9]

Experimental

General. All manipulations containing air- and moisture-sensitive compounds were carried out by the use of the standard Schlenk technique under argon atmosphere. All solvents were purified by distillation under argon after drying over calcium hydride or benzophenone ketyl. The chelating ligand pyphosH was prepared according to the literature.[38] Chromium(II) acetate (Aldrich) and potassium tetrachloroplatinate(II) (Wako) were used without further purification. $[PtCl_2(cod)_2]$, [PtClMe(cod)], and $[PtMe_2$-(cod)] were prepared according to the literature.[39] ^{1}H and

$^{31}P\{^1H\}$ NMR spectra in solution were recorded on a JEOL EX-270 and a GXS-270 operating at 270 (^1H NMR) or 109 MHz ($^{31}P\{^1H\}$ NMR) using 5 mm NMR tubes. $^{31}P\{^1H\}$ NMR was measured against external 85% H_3PO_4. Mass spectrometric data were obtained using FAB techniques on a JEOL SX-102 spectrometer by using 3-nitrobenzyl alcohol as a matrix and ESI techniques on a PE-Sciex API-III plus by dissolving the sample in dichloromethane. UV-vis spectra were taken on a Jasco V-570 in a sealed 2mm cell. Elemental analysis was performed at Graduate School of Engineering Science, Osaka University. All melting points were measured in sealed tubes and were not corrected. Crystallographic data collections and structure determination of **1** and **2** were already deposited.[6]

Preparation of $[Cr_2(pyphos)_4]$ (1). A reaction mixture of pyphos–Na (2.017 g, 6.7 mmol) and chromium(II) acetate (0.613 g, 1.63 mmol) in ethanol (40 mL) was stirred for 24 h to result in the precipitation of pale orange powders, which was separated by filtration. Recrystallization of the resulting solid from a mixture of dichloromethane and diethyl ether afforded **1** as orange crystals in 57% yield, mp 159–160 °C (dec). ^1H NMR (270 MHz, 30 °C, $CDCl_3$): δ 5.94 (1H, d, J = 8 Hz), 6.23 (1H, d, J = 7 Hz), 7.03 (1H, t, J = 7 Hz), 7.24–7.33 (10H, m); ^{31}P NMR (109 MHz, 30 °C, $CDCl_3$): δ –4.3 (br, fwhm = 660 Hz); UV-vis (CH_2Cl_2): 275 (ε 3.7 × 10^4), 330 (ε 2.1 × 10^4), 455 nm (ε 4.7 × 10^2). μ_{eff} = 1.70 B.M. (25 °C). MS (FAB) m/z 1217 (MH^+). Anal. Found: C, 63.87; H, 4.12; N, 4.36%. Calcd for $C_{60}H_{52}N_4O_4P_4Cr_2{\cdot}CH_2Cl_2$: C, 63.65; H, 4.18; N, 4.30%.

Preparation of $[Cr_2Pt_2Me_4(pyphos)_4]$ (2). A mixture of complex **1** (0.142 g, 0.11 mmol) and $PtMe_2$(cod) (0.074 g, 0.22 mmol) in THF (20 mL) was stirred for 3 h at –70 °C and then warmed up to room temperature gradually. Removal of all volatiles left **2** as an orange solid in quantitative yield. The resulting solid was recrystallized from a mixture of THF and diethyl ether to afford complex **2** as red cubic crystals, mp > 300 °C. NMR spectroscopy in solution displayed no signals due to the paramagnetism of the product; however, in solid state, signals due to phosphorus nuclei could be observed (vide infra). UV-vis (CH_2Cl_2): 303 (ε 1.7 × 10^4), 386 nm (ε 9.0 × 10^3). MS (ESI): m/z 1668.1 (MH^+). Anal. Found: C, 53.17; H, 4.72; N, 3.05%. Calcd for $C_{72}H_{64}Cr_2N_4O_4P_4Pt_2{\cdot}2(C_4H_{10}O)$: C, 52.92; H, 4.66; N, 3.09%.

Preparation of $[Cr_2Pt_2Cl_4(pyphos)_4]$ (3). A mixture of complex **1** (0.090 g, 0.07 mmol) and $PtCl_2$(cod) (0.052 g, 0.14 mmol) in dichloromethane (20 mL) was stirred for 24 h; the color changed from yellow to green. A few precipitated solids were removed by centrifugation and the solution was concentrated in vacuo to yield powder of **3** in quantitative yield. Recrystallization from a mixture of dichloromethane and diethyl ether afforded complex **3** as red needle crystals, mp > 300 °C. ^1H NMR (270 MHz, 30 °C, $CDCl_3$) δ 6.50 (1H, br), 6.80 (1H, br), 7.27–7.57 (11H, m). ^{31}P NMR (109 MHz, 30 °C, $CDCl_3$) δ 12.6 (J_{Pt-P} = 3590 Hz). MS (FAB) m/z 1607 (M^+ – 4Cl). UV-vis (CH_2Cl_2) 275 (ε 2.5 × 10^4), 310 nm (ε 2.3 × 10^4). Anal. Found: C, 43.62; H, 3.80; N, 2.86%. Calcd for $C_{68}H_{52}Cl_4Cr_2N_4O_4P_4Pt_2{\cdot}2(CH_2Cl_2)$: C, 43.82; H, 2.94; N, 2.92%.

Preparation of $[Cr_2(PtClMe)_2(pyphos)_4]$ (4). PtClMe(cod) (0.08 g, 0.08 mmol) in THF (20 mL) was added very gently to a solution of complex **1** (0.05 g, 0.04 mmol) in dichloromethane (20 mL) so as to maintain a THF/dichloromethane interface. After 2 weeks, slow diffusion of THF solution into the dichloromethane solution produced orange needle crystals of **4** quantitatively. Complex **4** is insoluble in common organic solvents, mp > 300 °C. ^1H NMR (270 MHz, 30 °C, $CDCl_3$) and $^{31}P\{^1H\}$ NMR (109 MHz, 30 °C, $CDCl_3$) in solution were not measured due to low solubility of **4**. MS (FAB) m/z 1672 (M^+ – Cl). UV-vis (CH_2Cl_2): 298.0 (ε 2.8 × 10^4), 432.5 nm (ε 2.4 × 10^3). Beilstein method: positive. Anal. Found: C, 48.67; H, 3.53; N, 3.24%. Calcd for $C_{70}H_{58}Cl_2Cr_2N_4O_4P_4Pt_2$: C, 49.22; H, 3.42; N, 3.28%.

Magic Angle Spinning NMR at Variable Temperatures. Magic angle spinning ^{31}P NMR spectra were measured by a single pulse method with proton decoupling at the magic angle spinning speed of 5–15 kHz with Bruker DSX300 spectrometer between 160 K and 350 K. $\pi/2$ pulse length was 4 μs for both ^{31}P and ^1H nuclei. The number of accumulations was between 450 and 1800 and the repetition time was 4 s. The shift was measured from 85% H_3PO_4 and external reference of $NH_4H_2PO_4$ (1.00 ppm) was used.[40]

A conventional zirconia rotor (4 mm) with boron nitride cap was used. The specimen (ca. 10–30 mg) was carefully packed at the center of the rotor (less than 4 mm long) to achieve homogeneous temperature at the sample position and Teflon powder was used as spacers. Sample preparation was performed in a glove box filled with dry nitrogen gas and the rotor was quickly transferred to the CP/MAS NMR probe through the Bruker sample guide tube. Dry nitrogen gas evaporated from the liquid nitrogen container was used as bearing and driving gas for the magic angle spinning. No decomposition of the sample was detected during the measurements.

The thermometer of the MAS NMR probe was carefully calibrated against the isotropic chemical shift of ^{207}Pb-MAS NMR spectrum of $[Pb(NO_3)_2]$[41] and the solid–solid phase transition temperatures of cyclooctanone ($C_8H_{14}O$, T_t = 227 K) and diazabicyclooctane ($(C_2H_4)_3N_2$, T_t = 350 K), which were determined by ^1H-MAS NMR, as previously reported.[42] The uncertainty of the temperature measurement after the calibration was 4 K and the temperature fluctuation during the accumulation of the NMR signals was within 2 K.

Magnetic Measurement by a SQUID Magnetometer. The temperature dependence of magnetic susceptibilities of complex **1–4** were measured by a SQUID magnetometer (Quantum Design MPMS-5S). The samples of **1–4** were measured in a sealed tube containing a little He gas between 40 and 400 K.

We thank Dr. S. Takamizawa for his assistant to magnetic measurement. We are grateful to the Ministry of Education, Science, Sports and Culture (the Grant-in-Aid for Scientific Research on Priority Areas) for the financial support.

References

1 F. A. Cotton and R. A. Walton, "Multiple Bonds Between Metal Atoms," Oxford Univ. Press, New York (1993).

2 F. A. Cotton, H. Chen, L. M. Daniels, and X. Feng, *J. Am. Chem. Soc.*, **114**, 8980 (1992).

3 F. A. Cotton and G. G. Stanley, *Inorg. Chem.*, **16**, 2668 (1977).

4 D. M. Collins, F. A. Cotton, and C. A. Murillo, *Inorg. Chem.*, **15**, 1861 (1976).

5 F. A. Cotton and W. T. Hall, *Inorg. Chem.*, **16**, 1867 (1977).

6 K. Mashima, M. Tanaka, K. Tani, A. Nakamura, W. Mori, S. Takeda, and K. Yamaguchi, *J. Am. Chem. Soc.*, **119**, 4307 (1997).

7 F. A. Cotton, P. E. Fanwick, R. H. Niswandew, and J. C. Sekutowski, *J. Am. Chem. Soc.*, **100**, 4725 (1978).

8 F. A. Cotton, L. M. Daniels, C. A. Murillo, I. Pascual, and

H.-C. Zhou, *J. Am. Chem. Soc.*, **121**, 6856 (1999).
9 F. A. Cotton, C. A. Murillo, L. E. Roy, and H.-C. Zhou, *Inorg. Chem.*, **39**, 1743 (2000).
10 F. A. Cotton and T. Ren, *J. Am. Chem. Soc.*, **114**, 2237 (1992).
11 F. A. Cotton, R. H. Niswander, and J. C. Sekutowski, *Inorg. Chem.*, **18**, 1152 (1979).
12 F. A. Cotton, W. H. Ilsley, and W. Kaim, *Inorg. Chem.*, **19**, 1453 (1980).
13 F. A. Cotton, C. E. Rice, and G. W. Rice, *J. Am. Chem. Soc.*, **99**, 4704 (1977).
14 M. Kranz and A. Witkowska, *Inorg. Synth.*, **6**, 144 (1960).
15 F. A. Cotton and T. R. Felthouse, *Inorg. Chem.*, **19**, 328 (1980).
16 M. Krumm, B. Lippert, L. Randaccio, and E. Zangrando, *J. Am. Chem. Soc.*, **113**, 5129 (1991).
17 M. Krumm, E. Zangrando, L. Randaccio, S. Menzer, and B. Lippert, *Inorg. Chem.*, **32**, 700 (1993).
18 J. J. Novoa, G. Aullon, P. Alemany, and S. Alvarez, *J. Am. Chem. Soc.*, **117**, 7169 (1995).
19 M. C. Grossel, J. R. Batson, R. P. Moulding, and K. R. Seddon, *J. Organomet. Chem.*, **304**, 391 (1986).
20 A. L. Balch, B. C. Noll, M. M. Olmstead, and D. V. Toronto, *Inorg. Chem.*, **32**, 3613 (1993).
21 C. Mealli, F. Pichierri, L. Randaccio, E. Zangrando, M. Krumm, D. Holtenrich, and B. Lippert, *Inorg. Chem.*, **34**, 3418 (1995).
22 A. L. Balch and V. J. Vatalano, *Inorg. Chem.*, **30**, 1302 (1991).
23 A. L. Balch, B. C. Noll, M. M. Olmstead, and D. V. Toronto, *Inorg. Chem.*, **31**, 5226 (1992).
24 A. Blagg, B. L. Shaw, and M. J. Thrnton-Pett, *J. Chem. Soc., Dalton Trans.*, **1987**, 769.
25 H. M. McConnell and D. B. Chesnut, *J. Chem. Phys.*, **28**, 107 (1958).
26 R. J. Kurland and B. R. McGarvey, *J. Magn. Reson.*, **2**, 286 (1970).
27 R. E. Carlin, "Magnetochemistry," Springer-Verlag, New York (1986).
28 G. N. La Mar, W. DeW Horrocks Jr., and R. H. Holm, "NMR of Paramagnetic Molecules, Principles and Applications," Academic Press, New York (1973).
29 G. N. La Mar, G. R. Eaton, R. H. Holm, and F. A. Walker, *J. Am. Chem. Soc.*, **95**, 63 (1973).
30 M. Nishino, M. Tanaka, S. Takeda, K. Mashima, W. Mori, K. Tani, A. Nakamura, and K. Yamaguchi, *Mol. Cryst. Liq. Cryst.*, **286**, 193 (1996).
31 M. Nishino, M. Tanaka, S. Takeda, K. Mashima, W. Mori, K. Tani, A. Nakamura, and K. Yamaguchi, *Mol. Cryst. Liq. Cryst.*, **286**, 201 (1996).
32 M. Nishino, S. Yamanaka, Y. Yoshioka, and K. Yamaguchi, *J. Phys. Chem.*, **A 101**, 705 (1997).
33 L. Bennes, J. Kalousova, and J. Votinsky, *J. Organomet. Chem.*, **290**, 147 (1985).
34 M. H. Chisholm, F. A. Cotton, M. W. Extine, and D. C. Rideout, *Inorg. Chem.*, **17**, 3536 (1978).
35 F. A. Cotton, M. W. Extine, and G. W. Rice, *Inorg. Chem.*, **17**, 176 (1978).
36 F. A. Cotton, B. G. DeBoer, M. D. LaPrade, J. R. Pipal, and D. A. Ucko, *Acta Crystallogr., Sect. B*, **27**, 1644 (1971).
37 K. Mashima, H. Nakano, and A. Nakamura, *J. Am. Chem. Soc.*, **118**, 9083 (1996).
38 G. R. Newkome and D. C. Hager, *J. Org. Chem.*, **43**, 947 (1978).
39 H. C. Clark and L. E. Manzer, *J. Organomet. Chem.*, **59**, 411 (1973).
40 S. Hayashi and K. Hayamizu, *Bull. Chem. Soc. Jpn.*, **62**, 2429 (1989).
41 A. Bielecki and D. P. Burum, *J. Magn. Res.*, **A116**, 215 (1995).
42 G. Maruta, S. Takeda, R. Imachi, T. Ishida, T. Nogami, and K. Yamaguchi, *J. Am. Chem. Soc.*, **121**, 424 (1999).